Developments, Applications and Tutorials in Experimental Mechanics Techniques
EXPERIMENTAL TECHNIQUES SEM

# Flexible Rod Design for Educational Wind Balance



| | |
|---|---|
| Journal: | *Experimental Techniques* |
| Manuscript ID: | EXT-T-0930.R1 |
| Manuscript Type: | Technical Article |
| Date Submitted by the Author: | n/a |
| Complete List of Authors: | Raush, Gustavo; Universitat Politècnica de Catalunya, Fluid Mechanics<br>Castilla, Roberto; Universitat Politècnica de Catalunya, Fluid Mechanics<br>Gamez-Montero, Pedro Javier; Universitat Politècnica de Catalunya, Fluid Mechanics<br>Wojciechowski, Jan; Technical University of Warsaw, Institute of Aeronautics and Applied Mechanics<br>Codina, Esteve; Universitat Politècnica de Catalunya, Fluid Mechanics |
| Keywords: | Fluid Mechanics, Joints and Connections, Instruments, engineering education, Mechanical |
| Topic : | Sensors and Instrumentation |
| | |

# Flexible Rod Design for Educational Wind Balance

G. Raush* R. Castilla P. J. Gàmez-Montero
J. Wojciechowski E. Codina

LABSON, Department of Fluid Mechanics
Universitat Politècnica de Catalunya
Terrassa Spain



**Abstract**

*This article provides a technical description of a flexible hinge for wind tunnel rigs. For academic purposes, the device was integrated into several rod flexures to build a home-made external wind balance system. The cylindrical elastic element incorporates several notches, and the flexure linkage is able to transmit force in the main axial direction without hindering perpendicular movement. The flexural element described here is simple and easily manufactured, and can also be used with other types of wind balance. The flexure described in this article has similar functionality to those mentioned in the reference section, but has a more compact element. The project's effectiveness was demonstrated in a series of experimental comparisons of forces and moments measured on a wing using the N.A.C.A. Clark-Y airfoil profile.*

***Keywords***: *flexure, flexible hinge, wind tunnel balance, Clark Y airfoil, force & moment measurement*

*corresponding author: gustavo.raush@upc.edu

# Nomenclature

$\mathbf{a}, \mathbf{b}, \mathbf{c}, \mathbf{d}, \mathbf{e}, \mathbf{f}$ : Direct measured forces, (N)

$A$ : Cross sectional area of the column, ($m^2$)

$\alpha$ : angle of attack, (deg)

$AR$ : Aspect ratio of the airfoils (-)

$C_z$, $C_x$, and $C_p$ : Lift, drag and pitching moment coefficients at the tested airfoil, respectively

$D$, $L$, $S$ : Drag, Lift and Side force, respectively. (N)

$\Delta_y$ : Lateral deflection, (m)

$E$ : Modulus of elasticity

$J$ : Second moment of area, ($m^4$)

$K_\theta$ : Elastic constant, (Nm/rad)

$l$, $m$, $n$ : Rolling, pitching and yawing moments, respectively. (Nm)

$L_c$ : Length of the column, (m)

$P_{Ecr}, P_{Jcr}$ : Euler and Johnson critical loads, respectively.

$r_g$ : Radius of gyration, (m)

$S_r$ : Slenderness ratio

$\sigma_y$ : Yield strength, (Pa)

$x, w$ : dimensional parameters, (m)

# 1 Introduction

The wind tunnel is an essential tool for teaching aerodynamics in fluid mechanics and aeronautics courses [1, 2]. Many of its applications allow the measurement of aerodynamic forces exerted over bodies and flow visualizations to measure other elements [3]. Force measurement is an important issue, especially when the aim is to establish the wind profile's characteristics. One example of this is wind turbine blade performance carried out on experimental rigs [4]. Wind balances measure the steady and fluctuating forces that appear across bodies immersed in the fluid stream. Aerodynamic loads can be calculated with balance geometry and load measurements. After decoupling the interacting forces, loads over the model can be represented by six main quantities, three forces and three moments. A reliable wind balance at aerodynamic tunnel facilities is essential for these measurements to be accurately made.

Wind balances can be divided into strain gage, rotary, internal and external [5]. The internal balance is usually a stinger. Smith et al [6] describe an internal balance device used to measure six quantities (three forces and three moments). These kinds of instruments must be attached near the gravity center of the models [7]. The model must possess a minimum volume to allow internal balance [8, 9].

In special circumstances, the shape and dimensions of the model do not allow the use of an internal balance, for instance when testing small-scale airfoils or models. Engineering undergraduates are often required to build their own models during the course of their studies. Due to time and financial limitations, these homemade models cannot be very large, and external balances are fitted to house small prototypes. Furthermore, their open designs are highly educational, making them ideal for teaching purposes.

Four types of external balances are commonly used. They are classified according to their load-carrying categories [5, 10]: wire, platform, yoke and pyramidal, according to the manner in which the system is assembled. The platform balance is one of the most widely used and extensively documented (see reference section). Its working principle is based on the measurement of six principal forces, three in a vertical direction and the others horizontal. Load cells are used as force-sensing elements based on the strain gage deformation sensors. The force connections between the model and the strain gage cells are achieved using a set of long slender rods fixed to a floating rigid structure. This rigid piece is connected to the load cells by specialized

flexible elements that serve as elastic hinges. These hinges play an important role, ensuring that the set formed by the model and its supports can be considered a free-floating body. Anther equally important issue is guaranteeing orthogonality between the forces transmitted to the load sensors. Usually, three rods are used to attach the model to the floating platform.

When the test model has an elongated shape and considerable aspect ratio like a streamlined body, the external balance is particularly suitable and allows the scaled airfoil to be directly fixed to the acting force struts. In an external wind balance, the strut rods play a vital role, transmitting aerodynamic forces to the sensor elements. Strut behavior should be able to withstand a large axial load but have very low resistance to lateral loads. Milling machined flexures with two perpendicular planes have been documented [5, 11]. The flexure sections are tuned according to the anticipated aerodynamic strength range. A compromise decision must be made between the axial load capacity and the flexibility needed with negligible reaction forces [11]. In this case there is a risk of buckling. If the strut rod is overloaded, further recalibration of the balance is required due to the permanent deformation suffered by the flexure. One solution would be to restrict the lateral displacement of the flexure by means of mechanical limits.

This article presents a patented flexible hinge, also known as a flexure, which has overcome the weak flexibility experienced in machining flexures which use thin elastic sheets. Section 2 briefly describes the underlying theory of wind balance principles. Section 3 presents a brief description of the theory behind the flexure's design. Section 4 describes the innovative solution, including its design details and authors. Finally, Section 5 presents several experimental tests on a Clark Y airfoil which show slightly different results to other previously published experimental data [12].

## 2 Wind Balance Details

Normally the external platform balances have three supports to host the airfoil being tested, see Fig. 6. This set is supported over a mainframe that exerts six decoupled forces on the load cells hosted at the base of the structure. The equations below show the aerodynamic forces and torques experienced by the aerodynamic body surrounded by the free flow. Further details can be found in [5].

$$L = -(\mathbf{a} + \mathbf{b} + \mathbf{c}) \quad (1)$$

$$D = \mathbf{d} + \mathbf{e} \quad (2)$$

$$S = -\mathbf{f} \quad (3)$$

$$l = (\mathbf{a} - \mathbf{b}) \left(\frac{1}{2} w\right) \quad (4)$$

$$n = (\mathbf{e} - \mathbf{d}) \left(\frac{1}{2} w\right) \quad (5)$$

$$m = \mathbf{c}\, x \quad (6)$$

Let $x$, $w$ be dimensional parameters. The equation system above is only valid if the force orthogonality is conserved. When large aerodynamic forces are omitted from the model, several unbalanced moments will be noted in the event of misalignments in actuating sensor strength. This drawback must be overcome using fine alignment followed by an accurate calibration procedure to remove the moment interactions.

## 2.1 Balance Linkages

The most important components of the external balance are the linkages designed to have minimum deflection under maximum loads. A noticeable number of them may be present in a balance test. The joint between the linkages and the platforms are the pivots that yield very small angular motion with negligible displacements. The pivots must allow only very low friction to avoid hysteresis in the balance when the loads revert their directions. The oldest balance models used knife edges [5, 13], experience drawn from the old analytical balance being of extreme importance. The knife edge is not suited to absorb shock loads and can only be used to transmit forces in the direction of compression; it does not allow pulling. For this reason knife pivots are usually replaced with flexible elements.

The flexible pivots have several advantages:

- frictionless minimized bearings.
- easy and cheap to manufacture.
- negligible hysteresis effects when the working limits do not overcome the elastic zone.
- high resistance to damage under normal conditions due to monolithic design.

- permanent damage only occurs after considerable rough treatment.
- loads from any directions may be measured with negligible interaction between components.

The outer part of the floating frame is held in place by a system of struts that are highly resistant to tension and compression, but are very easily bent. These struts must be long enough to reach out of the test section of the main balance's body and thin enough to avoid excessive interference with the main airstream. One of the most troublesome problems of wind tunnel balances is a lack of rigidity. The largest source of deflection is the mounting system. The force transmission must be ensured with null deflection in all directions except the direction of interest. Misalignments and deformations in undesired directions jeopardize the whole concept of orthogonality in the decoupled equation system previously described. The ideal system must allow a straightforward axial transmission of aerodynamic force to the load cell sensor without suffering any kind of beam deflection.

# 3 Design Overview

Flexible bearings and elastic hinges are a specialized application of bending theory. The principles of a buckling structure mechanism are modeled using differential equations of varying complexity [14, 15, 16]. Several types of behavior can be observed when structural elements are under compression [14]. The formulation and solution of these systems is beyond the scope of this article but a complete compendium of resolved application cases can be found in [17]. The number of feasible designs and applications is very large. Wang [11] reported the design of several flexible hinges where the behavior of different cross-sectional designs was analyzed. Zhu and Zhang [18] present the use of a monolithic flexure frame as a design strategy to reduce the total number of mechanical components. Slocum [19] highlights the design fundamentals of monolithic devices, detailing a flexible mount based on a cantilever element to be used in optical appliances.

Usually, the elements of flexible rods for external aerodynamic balances are made using mutually perpendicular flexible sheets joined at adjacent edges, as detailed in [5]. Damage caused by bending or twisting is the most commonly observed flaw in this design. Geometrics play a crucial role in solving this problem. If the length-width ratio is too small the element will be

crushed by the excessive yield strength created by compression, or buckling will occur. Buckling can be catastrophic and occur at any moment, making it a particularly dangerous flaw. The structural system collapses, often resulting in partial destruction of the balance, and unlike yielding failures, there may be no warning signs. Design engineers must therefore be particularly vigilant and always check buckling risk. Although based on the principles shown in [5], our idea has been improved to minimize the risk of buckling.

The next paragraphs describe the principles followed by designers to obtain a flexible element to be applied in aerodynamic balances. Our proposal, designed for academic purposes, is based on the construction of flexible elements as a single monolithic piece.

The loading conditions to consider are simple compression and bending. Traditional buckling analysis is based on Euler's theory. Stable column analysis is based on the use of free-pinned joints [17]. In this case, the most conservative critical load which will bring about column collapse is given by,

$$P_{Ecr} = \frac{\pi^2 \cdot E \cdot J}{2\, L_c^2} = \frac{\pi^2 \cdot E \cdot A}{2\, S_r^2} \tag{7}$$

or its equivalent yield stress

$$\sigma_{Ecr} = \frac{P_{Ecr}}{A} = \frac{\pi^2 \cdot E \cdot J}{2\, L_c^2 A} = \frac{\pi^2 \cdot E}{2\, S_r^2} \tag{8}$$

The slenderness ratio is defined as $S_r = L_c/r_g$ where $r_g$ is the radius of gyration, and is defined as $r_g = \sqrt{J/A}$ which is a parameter that measure the propensity of failure in a certain direction that of the least radius of gyration. Again $J$ is the second moment of area, and $A$ is the cross-sectional area of the column. Therefore the radius of gyration is $J = r_g^2\, A$. If the slenderness ratio $S_r > S_{cr}$ critical slenderness ratio, then the column is treated as a long column and the Euler buckling formula is applied,

$$S_{cr} = \sqrt{\frac{\pi^2 \cdot E}{\sigma_y}} \tag{9}$$

If $S_r < S_{cr}$ the column is treated as a short column. At this kind of column, failure may occur by compression without significant buckling and at stresses exceeding proportional limit. For this condition, Johnson's formula is used,

$$P_{Jcr} = \sigma_y A \left[1 - \left(\frac{\sigma_y}{4\pi^2 E}\right)\left(\frac{L_c}{r_g}\right)^2\right] \tag{10}$$

or the yield stress is determined by the following equation:

$$\sigma_{Jcr} = \sigma_y \left[1 - \left(\frac{\sigma_y}{4\pi^2 E}\right) S_r^2\right] \tag{11}$$

The limit condition to decide when expression (10) should be applied is obtained by solving the system formed by expressions (8) and (11). For $S_r \approx 20$, equation (10) could be approximated to a near pure compression $P_{cr} = \sigma_y A$. More accurate models and specific designs can be found in [19]. In following section the authors present a general overview of the design comparisons between the flexure presented in this article and other equivalent product available on the market.

Finally, the elastic constant experienced at the flexure head must be evaluated. Its value should be minimized in accordance with the axial load responsible for bending. The elastic constant $K_\theta$ depends on the lateral deflection $\Delta_y$ of flexure due to the lateral force aligned with direction with lowest $r_g$.

The column's lateral deflection $\Delta_y$ at $P$ axial load, solved by [17, 20] is given by,

$$\Delta_y = \frac{W\left[1 - \cos\left(\alpha L_c\right)\right] L_c}{P\cos\left(\alpha L_c\right)} - \frac{\left[L_c - \frac{\sin(\alpha L_c)}{\alpha}\right] W}{\alpha E J \cos\left(\alpha L_c\right)} \tag{12}$$

where $\alpha^2 = P/\left(EJ\right)$

For a given torque $\tau = W L_c$, the deflection $\Delta_y$ at the top of the column is evaluated by the angle $\theta = \Delta_y / L_c$ then,

$$K_\theta = \frac{W L_c^2}{|\Delta_y|} \tag{13}$$

The design procedure can be summarized by:

1. The maximum axial load $P_{Ecr}$ that will be transmitted over the load cell is set.

2. The designer sets the minimum achievable thickness of the flexure device. This issue is closely related to the machining method chosen and manufacturing technology applied.

3. From a pure compression hypothesis, the rectangular shaped column area gives the transverse width, and the minimum width will then be known.

4. The $S_{cr}$ is determined

5. With $J$ and $S_{cr}$ the column length $L_c$ could be estimated.

6. Using expression (12) the $K_\theta$ elastic constant may be known

7. If the design parameters $K_\theta$ do not verify the desired specifications, parameters like $L_c$ or $A$ could be modified, repeating the procedure from point 2.

# 4 Description of the Device

The flexible hinge [21] proposed here is made from a boring rod section, conveniently mechanized with several arc-shaped cuts. In order to achieve this, an appropriately-sized stainless steel tube is made using electrical discharge machining techniques, to make four thin cuts along the tube axis, see Fig. 1 and 3. This procedure creates two sets of symmetrical flat twin columns, which are able to withstand axial loads. This flexure design is based on folding the traditional flat pinned texture along the main axis, see [5]. The resulting flexible hinge overcomes the risk of buckling. The proposed design also permits the creation of a shorter flexible hinge, which is less prone to collapse in the event of a large axial force overload.

The proposed design [21] has several advantages over the traditional elastic foil [5]. First, the main structure itself limits the total lateral displacement that each column can perform. Secondly, axial misalignment between orthogonal planes is prevented by the accuracy of the machining procedure. Finally, the folding idea detailed here achieves more compact flexible struts, which could be used not only for wind balances but also other mechanical movement, such as those in optical positioning systems. Fig. 2(b) shows a cross section view of the flexure element with flat, flexible beam elements. Furthermore, the cuts are finished with short curvilinear segments in order to minimize stress concentration. Figure 3 shows the two threaded holes needed to fix the flexure to the platform or load cell.

Since the size of the flexible beam can be increased to deal with very high loads, the tested prototype was adapted to the wind tunnel available at the

department's facilities. The maximum loads are estimated in accordance with the highest anticipated aerodynamic forces at the facilities. The experimental test shows that the prototype achieves high linearity without appreciable hysteresis in the measurement of low loads such as those deployed on a small airfoil at low Reynolds numbers. The prototype has a width of 0.3 mm and length of 16 mm on each flexible element. Sizing the 8 mm external diameter with a 3.2 mm bore, the flexible element has a 0.3 x 2.4 = 0.72 $mm^2$ cross-section. The transmitted axial load was limited up to 11 N without an appreciable bending effect. The cut gap's thickness is achieved by lateral displacement permitted by the strain gage deformation. Furthermore, negligible bending was observed when the described prototype was tested up to 32 N load. The elastic constant was fixed at 0.015 Nm/rad. Figure 4 shows a general view of the external platform balance with flexible rods transmitting aerodynamic forces to the load cells. Figure 5 shows mechanized flexures in the first plane, which measure one component of drag force. The flexure pair, which provides the lift component of the force is shown in the rear plane.

# 5 Experimental Comparisons

An external wind balance, designed to assist academic courses, was equipped with elastic rods built using several of the flexures described above. In order to validate its performance, a Clark-Y airfoil was chosen to compare balance performing. Figure 6 shows the airfoil cross-section by percentage of chord profile,[22, 23]. Reliable data has been published regarding the Clark-Y airfoil; for instance, Silverstein [12] conducted a detailed study of the Reynolds number range $1{\cdot}10^6$ to $9 \cdot 10^6$ on the airfoil chord dimension.

The comparison was made at 30 m/s of mainstream velocity; equivalent to dynamic pressure of 518 Pa obtained by a Pitot probe, and a $1.6{\cdot}10^5$ airfoil Reynolds Number was reached. To make a reliable comparison, the airfoil's aspect ratio, defined by the chord/length relation, should be preserved or corrected. Thus, a 3.15 aspect ratio of Clark Y airfoil with 0.08 m chord length and 0.252 m wingspan was tested.

Test data on a 4 by 24 inches rectangular Clark Y airfoil of an aspect ratio of 6 were chosen for comparison [12]. The measured characteristics have been corrected both using the respective aspect ratios following the Abbott et al. [22]. Silverstein [12] exposed similar procedure. The effect on the airfoil characteristics are given by the following formulas:

$$C_D' = C_D + \frac{C_L^2}{\pi}\left(\frac{1}{AR'} - \frac{1}{AR}\right) \tag{14}$$

$$\alpha' = \alpha + \frac{C_L}{\pi}\left(\frac{1}{AR'} - \frac{1}{AR}\right) \tag{15}$$

where $C_D'$ and $\alpha'$ correspond, respectively, to the drag coefficient and angle of attack (radians) of the wing of aspect ratio $AR'$ which corresponds with the N.A.C.A. reference.

Figure 7(a) shows both N.A.C.A. and test lift coefficients . There are slightly differences at the small positive angles and negative incidences. Agreements of 3% mean square error have been measured. The stall condition appears at the angle of incidence of $\alpha = 12^o$, see Fig. 7(a). This fact agrees with Marchman *et al* [25] that describes similar behavior between the lift and the angle of attack. The anticipation of the stall phenomena is a feature related with the lower Reynolds numbers.

At lower Reynolds numbers, the stall condition occurs at lower angles. Therefore, the experimental data reflects the stall condition at $\alpha = 12^o$, meanwhile the N.A.C.A. reference appears near of $\alpha = 17^o$, see Fig.7(a) . At the stall condition, the maximum lift coefficient of the test airfoil is$C_{L,\max} = 1.1$ at $\alpha = 11^o$ in the test airfoil and $C_{L,\max} = 1.23$ at $\alpha = 13^o$ with N.A.C.A. references. Similar differences are reported by [25].

The minimum drag coefficient of N.A.C.A. airfoil is $C_{D,\min} = 0.01$ centered at $\alpha = -6.2^o$ whereas the tested airfoil performed $C_{D,\min} = 0.03$ at $\alpha = -1^o$. The instrumental error should be the reasons of the difference found.

Even though this deviation, there are other interesting aspect to point out. Between the 13 to 17 degree interval of the angle of attack, the drag experiments a singular rise-up behavior. Very similar behavior has been observed in Marchman [25] when the authors compare low Reynolds drags against drags at the high Reynolds conditions.

Another characteristic which is of importance in the study is the curve of the lift to drag ratio plotted against angle. Particularly, the L/D characteristic shows the significant influence of the drag rise-up pointed above, see Fig. 8. Values of L/D ratio decrease with decrease of aspect ratio from 6 for the N.A.C.A. wing to 3.15 for the tested wing. Furthermore, the maximum L/D

coefficient shifts toward to bigger angles when the aspect ratio decreases. Similar behavior are reported by [24].

The pitching moment coefficient needs a more detailed analysis. There is a scale difference between both measurements but significant statistical correlations have been measured. A linear correlation analysis shows a scale factor of 1.63 with a 0.91 regression coefficient value taken from the normalized covariance matrix. The coincidence is quite relevant, as observed in Fig. 9(c).

Figure 9(a) shows the comparatives performances between pitching moment against lift. Regarding the differences shown by the linear regression, the pitching moment curve of the tested airfoil is below the N.A.C.A. reference due to the aspect ratio differences [24].

# 6 Conclusions

A flexible cylindrical bearing with a small elastic constant, specifically designed to build elastic prongs was presented. A platform wind balance for academic projects was the primary objective. The flexure is based on the idea of folding two perpendicular planes along the principal axis. Both planes act as a flat elastic element required for the balance struts. The compact flexible monolithic spring used as a wind balance may be extended to other micro-mechanical positioners.

In this article, a comprehensive description of the design procedure has been presented. Several comparisons have been carried out to test flexure performance, using performance data from the well-established N.A.C.A. Clark Y airfoil as a basis. Lift and drag forces, together with pitching moments have been measured after balance calibration. Based on the comparative experimental and reference data, slight differences have been found in the lift, drag and pitching moment. The device developed is an affordable option for building a wind platform balance for academic use. Due to its performance it is also suitable for other applications, such as optical positioning systems.

# References

[1] Hinojosa, F.Z., Design of a new wind tunnel facility at industrial engineering school in Badajoz (Spain), *In Fifth Int. Conf. on Advances in*

*Fluid Mechanics, AFM V,* 40, 397-404, Lisbon, 2004

[2] Morris, M., Post, S., Force balance design for educational wind tunnels, *Conf. Proc. of ASEE American Society for Engineering Education*, 2010

[3] Beck, T., Anderson, B., Hosni, M., A simple educational wind tunnel setup for visualization of duct flow streamlines and nozzle/diffuser boundary layer separation, *Report of Department of Mechanical and Nuclear Engineering*, Kansas State University (KSU), 2008

[4] Buckley, M., Wind tunnel tests on the 1/30th scale model of the 60M wind turbine generator, *Proc. of Wind Energy Workshop*, 96-108, Cranfield, England, 1980

[5] Barlow, J.B., Rae, W.H., Pope, A., *Low-speed wind tunnel testing*, Addison-Wiley, New York, 1999

[6] Smith, A.L. Mee, D.J., Daniel, W.J., Shimoda, T., Design, modelling and analysis of a six component force balance for hypervelocity wind tunnel testing, *Computers and Structures*, vol. 79, no. 11, 1077-1088, 2001

[7] Boyden, R.P., Johnson, W.G. Jr., Ferris, A.T., Aerodynamic Force Measurements With A Strain-gage Balance In A Cryogenic Wind Tunnel, *NASA Technical Paper*,1983

[8] Zhai J., Ewald B., Hufnagel K., Investigation on the interference of internal six-component wind tunnel balances with FEM, *ICIASF Record, International Congress on Instrumentation in Aerospace Simulation Facilities*, 16.1-16.10, 1995

[9] Wang, Y.-H., Zhao, Z.-L., Development of the interference force measurement balance for sub-missile, *Experiments and Measurements in Fluid Mechanics*, vol 19, num 1, pp 71-74, 2005

[10] Fan Z., Measurement of Aerodynamic Forces and Moments in Wind Tunnels, *Encyclopedia of Aerospace Engineering*, vol 70, 811-823, 2010

[11] Wang, T., Qiu, J., Liu, X., Definition measurement unit with flexure hinges for a wind tunnel balance, *IEEE Int. Conf. on Information and Automation (ICIA)* ICIA 2010, vol 24, num 1, 1457-1462, 2010

[12] Silverstein A., Scale effect on Clark Y airfoil characteristics from N.A.C.A. full-scale wind-tunnel tests, *N.A.C.A. Report 502*, 1935

[13] Gorlin S. M., Slezinger I. I., Wind Tunnels and Their Instrumentation, *Israel Program for Scientific Translations*, 599, 1966

[14] Brush, D.O., Almroth, B.O., *Buckling of Bars, Plates, and Shells*, McGraw-Hill (New York), 1975

[15] Timoshenko, S., Gere, J.M., *Theory of elastic stability*, McGraw-Hill (New York), 3rd Edition, 1970

[16] Ugural, A., Fenster, S., *Advanced Strength and Applied Elasticity*, Prentice Hall (New Jersey), 3rd Edition, 1995

[17] Young, W.C., Roark, R.J., Budynas, R.G., *Roark's formulas for stress and strain*, McGraw-Hill, McGraw-Hill's Engineering Serie, 2002

[18] Zhu Z., Zhang B., A Linear Piezomotor Integrated by a Monolithic Flexural Frame, *Journal of Mechanical Design*, vol 119, num 3, 414-416, 1997

[19] Slocum, A.H., *Precision machine design*, Prentice-Hall, 1992

[20] Xie, W.-C., *Differential Equations for Engineers*, Cambridge University Press, 2010

[21] Castilla, R., Gamez-Montero, P.J., Wojciechowski, J., Codina, E., Flexible Rod for Aerodynamic Platform Scales, *Pat. Num. WO/2008/129107*, UPC, 2008

[22] Abbott, I.H. and Von Doenhoff, A.E., Theory of Wing Sections (New York: Dover 1959)

[23] Selig, M.S, Donovan, J.F. and Fraser, D.B., Airfoils at Low Speeds, 1989

[24] Zimmerman, C.H., Characteristics of Clark Y airfoils of small aspect ratios, *N.A.C.A. Report 4*31, 1933

[25] Marchman, J. and Werme, T. Clark-Y Airfoil Performance at Low Reynolds Numbers, *AIAA 22nd Aerospace Sciences Meeting*, 1984

# Figures

## List of Figures


1 Schematic of the platform balance where the main forces and dimensional parameters are shown . . . . . 15
2 The flexure element . . . . . 16
3 Cross sectional view of flexure element . . . . . 17
4 General view of the wind platform balance with prongs integrated into flexures . . . . . 18
5 Detailed view of flexures inside prong to measure drag force . 19
6 Airfoil cross-section by percentage of chord profile . . . . . 19
7 Experimental and N.A.C.A. Reference comparisons of lift and drag coefficients . . . . . 20
8 $L/D$ ratio comparison between tested airfoil and N.A.C.A. Report . . . . . 21
9 Comparisons of pitching moment . . . . . 21


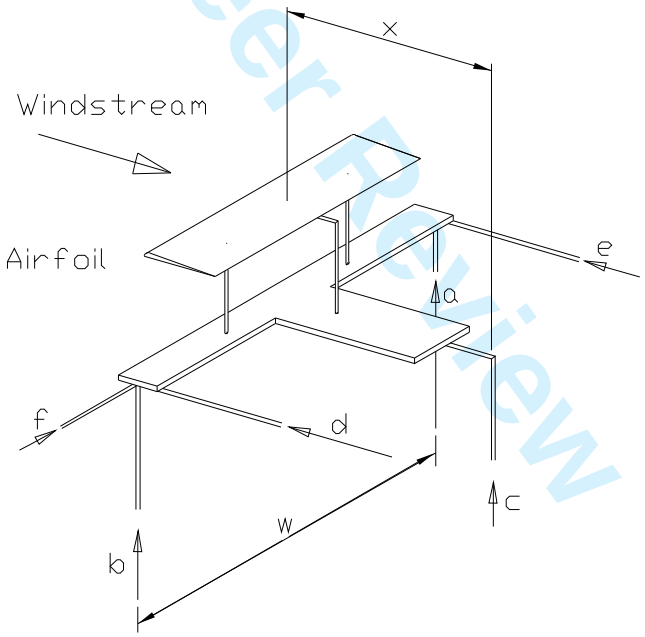


Figure 1: Schematic of the platform balance where the main forces and dimensional parameters are shown

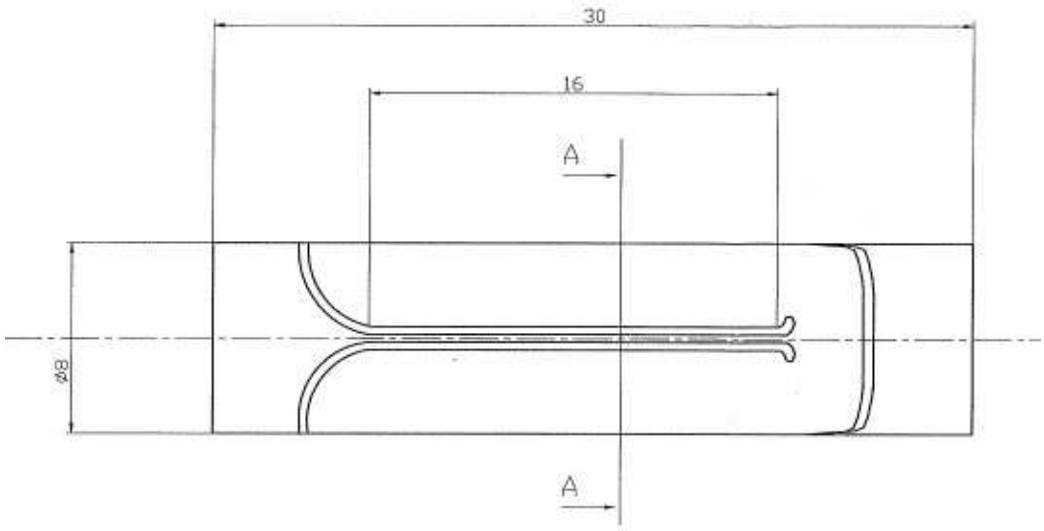


(a) Longitudinal view

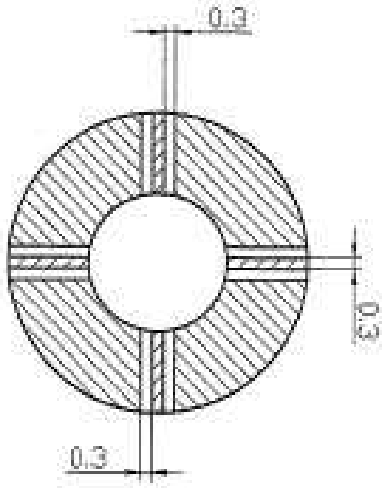


(b) Traversal cross sectional A-A view

Figure 2: The flexure element

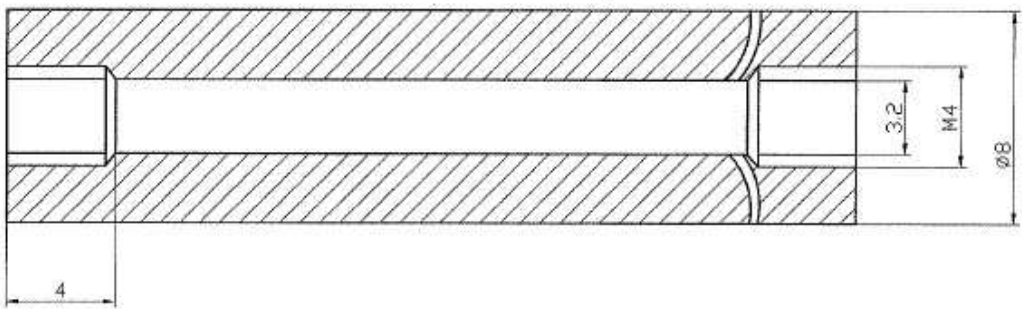


Figure 3: Cross sectional view of flexure element

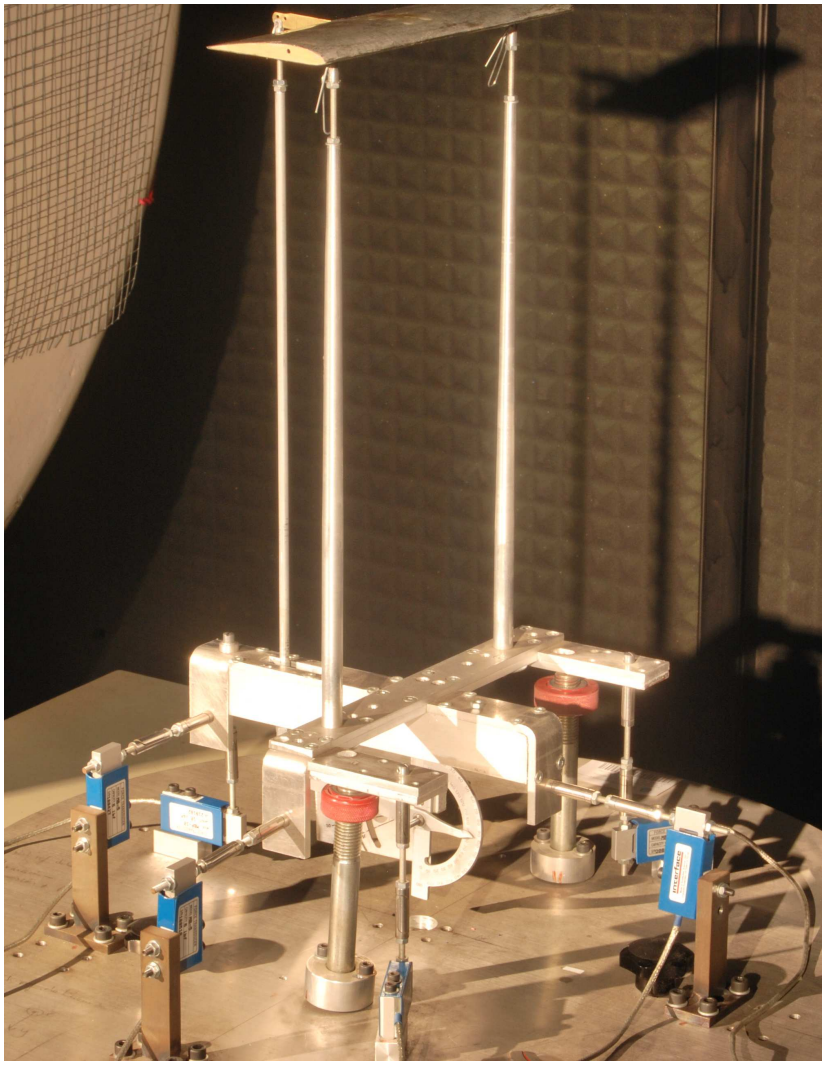

Figure 4: General view of the wind platform balance with prongs integrated into flexures

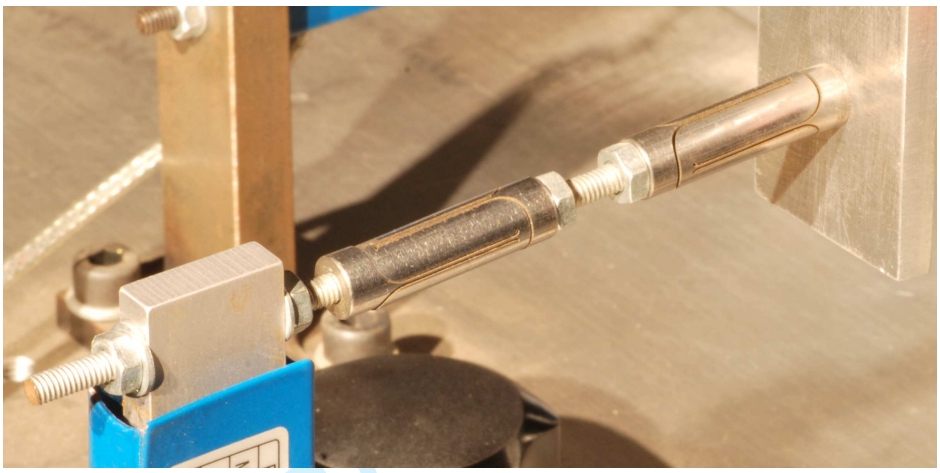

Figure 5: Detailed view of flexures inside prong to measure drag force

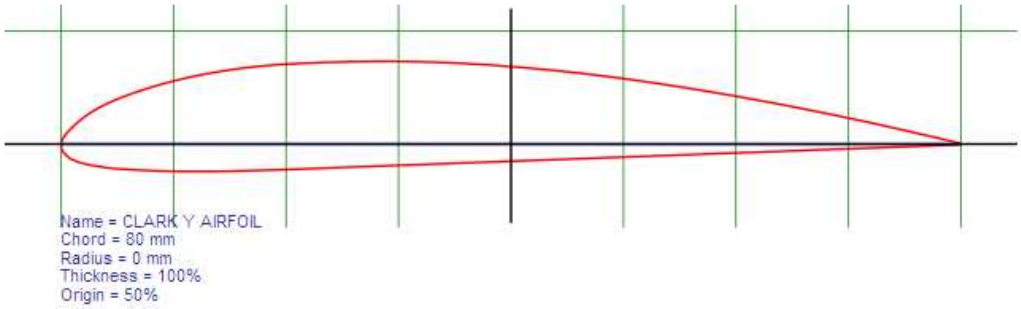


Figure 6: Airfoil cross-section by percentage of chord profile

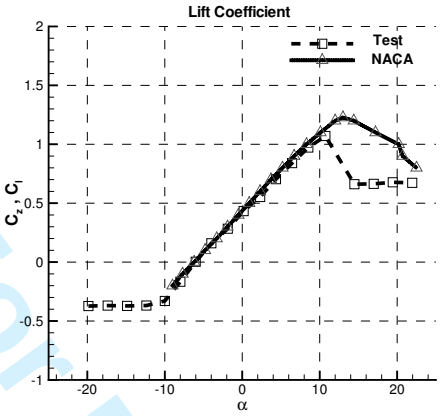


(a) Lift

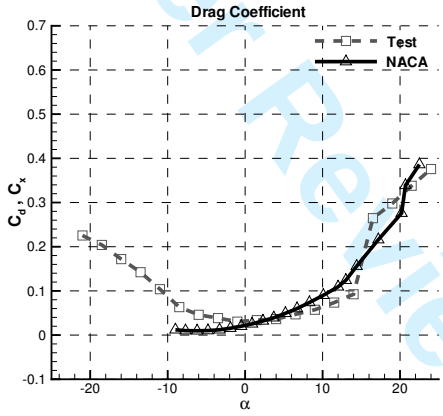


(b) Drag

Figure 7: Experimental and N.A.C.A. Reference comparisons of lift and drag coefficients

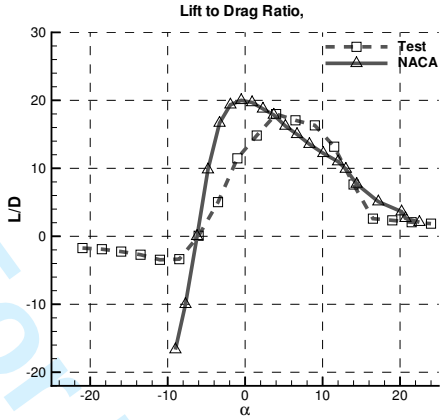


Figure 8: $L/D$ ratio comparison between tested airfoil and N.A.C.A. Report

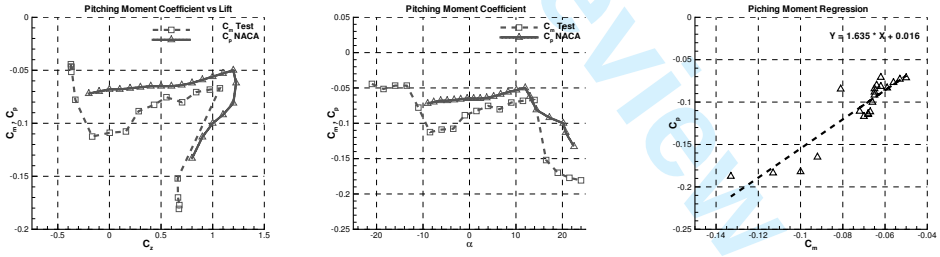


(a) Pitching - $C_D$ (b) Pitching - $\alpha$ (c) Linear Regression

Figure 9: Comparisons of pitching moment